Supplementary Information (SI) for Dalton Transactions.
This journal is © The Royal Society of Chemistry 2026

Supplementary Information

for

Magneto-structural correlations in cobalt(II)-phenanthroline compounds with chloranilic acid

by

Filip Torić,[a] Lidija Androš Dubraja,[a] Mirta Herak,[b] Nikolina Novosel,[b] Irina Petreska,[c] Krešimir Molčanov[a,*] and Dijana Žilić[a,*]

[a] Ruđer Bošković Institute, Bijenička cesta 54, 10000 Zagreb, Croatia.
[b] Institute of physics, Department for Research of Materials under Extreme Conditions, Bijenička cesta 46, 10000 Zagreb, Croatia.
[c] Ss. Cyril and Methodius University in Skopje, Faculty of Natural Sciences and Mathematics – Skopje, Institute of Physics, PO Box 162, 1000 Skopje, Macedonia.

E-mail: kresimir.molcanov@irb.hr, dijana.zilic@irb.hr

Contents

List of Figures

List of Tables

S1 Experimental

S1.1 Synthesis

[Co(phen)$_2$(CA)]·ROH. The aqueous solution (4 mL) of $CoCl_2 \cdot 6H_2O$ (23 mg; 0.1 mmol) was put into a test tube. Chloranilic acid (17 mg; 0.08 mmol) and phen (19 mg; 0.1 mmol) were dissolved in alcohol (8 mL, EtOH/MeOH) giving dark red coloured solution, which was carefully laid above the pink coloured aqueous solution. In the next two days dark red prismatic crystals started to appear near the contact area between aqueous and alcohol layers. Crystals were left to grow for the following 7 days, after which were removed from the test tube and dried in air. The yield was $\approx$ 70%. IR data (KBr, cm^{-1}) **[Co(phen)$_2$(CA)]·EtOH:** 3419 (m), 3068 (w), 2970 (w), 2921(w), 2852 (w), 1625 (w), 1581 (w), 1528 (vs), 1496 (m), 1427 (m), 1368 (m), 1345 (w), 1320 (w), 1308 (w), 1225 (w), 1212 (w), 1141 (w), 1103 (w), 1049 (w), 989 (w), 868 (w), 851 (m), 834 (m), 780 (w), 728 (m), 643 (w), 586 (w), 574 (m), 472 (w), 423 (w), 393 (w), 375 (w); **[Co(phen)$_2$(CA)]·MeOH:** 3445 (m, br), 3074 (w), 2957 (w), 2920 (m), 2851 (w), 1626 (w), 1582 (w), 1529 (vs), 1496 (m), 1427 (m), 1371 (m), 1347 (w), 1316 (w), 1308 (w), 1225 (w), 1212 (w), 1140 (w), 1103 (w), 1044 (w), 990 (w), 868 (w), 851 (m), 834 (m), 781 (w), 728 (m), 643 (w), 586 (w), 574 (m), 470 (w), 425 (w), 391 (w), 364 (w).

[Co(phen)$_2$(CA)]·H$_2$O. The yellow coloured aqueous solution (2 mL) of $CoCl_2 \cdot 6H_2O$ and phen (23 mg; 0.1 mmol) was put into a test tube, and violet coloured aqueous solution (8 mL) of chloranilic acid (17 mg; 0.08 mmol) was carefully laid above it. In the next two days dark red prism-like crystals started to appear near the contact area between two layers. The crystallization process was finished after one week. Crystals were then collected from the test tube and dried in air. The yield was $\approx$ 40%. IR data (KBr, cm^{-1}): 3455 (m, br), 3074 (w), 2994 (w), 2922 (w), 1625 (m), 1582 (w), 1529 (vs), 1494 (s), 1427 (m), 1371 (m), 1347 (w), 1307 (w), 1225 (w), 1213 (w), 1140 (w), 1103 (w), 1050 (w), 1034 (w), 1004 (w), 990 (w), 965 (w), 868 (w), 851 (m), 834 (m), 812 (w), 782 (w), 728 (m), 643 (w), 574 (w), 509 (w), 472 (w), 446 (w), 423 (w), 375 (w).

[Co(phen)$_2$(CA)]·EtGly. Ethylene glycol (2 mL) was used to dissolve $CoCl2 \cdot 6H_2O$ (23 mg; 0.1 mmol) and the pink coloured solution was put into a test tube. Chloranilic acid (17 mg; 0.08 mmol) and phen (19 mg; 0.1 mmol) were dissolved in 2 mL of H_2O and 4 mL of ethylene glycol, giving violet coloured solution, which was carefully laid above layer with $CoCl_2$. In the next two days dark red stick-like crystals started to appear near the contact area between two layers. Crystals were left to grow for the following 7 days, after which were removed from the test tube and dried in air. The yield was $\approx$ 40%. IR data (KBr, cm^{-1}): 3425 (m, br), 3065 (w), 2925 (w), 2854(w), 1624 (w), 1526 (vs), 1516 (vs), 1494 (s), 1426 (m), 1376 (m), 1344 (w), 1322 (w), 1225 (w), 1210 (w), 1142 (w), 1102 (w), 1089 (w), 1075 (w), 1048 (w), 1034 (w), 1022 (w), 1004 (w), 991 (w), 868 (w), 852 (m), 837 (m), 779 (w), 728 (m), 668 (w), 643 (w), 607 (w), 576 (m), 518 (w), 470 (w), 444 (w), 425 (w), 393 (w), 375 (w), 356 (w).

S1.2 Elemental analysis

Elemental analysis was performed at an Elemental Perkin Elmer instrument, 2400 Series II CHNSO Analyzer.

S1.3 X-ray diffraction

Single crystal measurements were performed on a dual source (Mo/Cu) Rigaku Oxford Diffraction Synergy S diffractometer equipped with an Oxford Cryosystems Series 800 cryostat. Program package CrysAlis PRO[1] was used for data reduction and absorption correction. The structures were solved using SHELXS97[2] and refined with SHELXL-2017[3]. Models were refined using the full-matrix least squares refinement; all non-hydrogen atoms were refined anisotropically. Hydrogen atoms were located in a difference Fourier map and refined either as riding entities or free, restrained entities. Molecular geometry calculations were performed by PLATON[4] and molecular graphics were prepared using ORTEP-3[5], and Mercury[6]. Crystallographic and refinement data for the structures reported in this paper are shown in Tables S1 and S2. Expressions for measures of octahedral distortion that are commonly used, ζ, Δ and Σ[7] are given with equations S1,S2 and S3.

$$\zeta = \sum_{i}^{6} |d_i - d_{mean}| \tag{S1}$$

$$\Delta = \frac{1}{6} \sum_{i}^{6} \left(\frac{d_i - d_{mean}}{d_{mean}} \right)^2 \tag{S2}$$

$$\Sigma = \sum_{i}^{12} |90^\circ - \theta_i| \tag{S3}$$

where, where d_i is individual M-X bond distance, d_{mean} is mean metal-ligand bond distance and θ_i is individual cis angle.

S1.4 Powder X-ray diffraction

The powder X-ray diffraction (PXRD) data were collected in reflection mode using Cu-Kα radiation (λ = 1.54060 Å) using a Malvern Panalytical Empyrean diffractometer with a step size of 0.013° in a 2θ range between 4° and 50°.

S1.5 ESR spectroscopy

The ESR measurements were performed on a Bruker Elexsys 580 FT/CW X-band spectrometer, ranging from room temperature to liquid helium temperature. The microwave frequency was approximately 9.7 GHz, with a magnetic field modulation amplitude of 0.5 mT and a modulation frequency of 100 kHz.

S1.6 Static magnetization measurements

The magnetization measurements were performed using the Quantum Design (QD) MPMS3 VSM-SQUID magnetometer in temperatures ranging from 1.8 K to 300 K and in magnetic fields of up to $\pm$7 T. The powder samples were mounted inside the standard QD VSM capsule and inserted into the standard QD brass sample holder. The signal from the empty capsules is diamagnetic and several orders of magnitude smaller than the signal from the samples.

S1.7 AC magnetic susceptibility measurements

AC magnetic susceptibility measurement in zero external DC magnetic field (with compensation of Earth's magnetic field) was recorded at the lowest possible temperature (1.3 K) using the CryoBIND system with the inductive technique. The measurements were performed in the driving-field frequency range of 1–1000 Hz and at an amplitude of 5.4 Oe. AC magnetic susceptibility measurements were performed in an applied static magnetic field using a Quantum Design MPMS3 magnetometer with an ac driving field of amplitude 2 Oe and frequencies in the range 1–1000 Hz.

S1.8 DFT calculation

DFT (density functional theory) calculations were carried out by using the Gaussian series of programming packages[8]. We used the hybrid functional B3LYP (Becke, 3-parameter, Lee-Yang-Parr) and the LANL2DZ (Los Alamos National Laboratory 2 Double-Zeta) basis set. The input geometries were adopted from the experimentally obtained crystallographic data at a temperature of 100 K.

S2 Results and discussion

S2.1 Elemental analysis

The powder samples were subjected to a microanalysis. Anal. Calcd. for **1**·MeOH: C, 56.55; H, 3.06; N 8.51. Found C, 53.10, H, 2.99; N 7.94. Anal. Calcd. for **1**·EtOH: C, 57.16; H, 3.29; N 8.33. Found C, 53.04, H, 2.87; N 7.22. Anal. Calcd. for **1**·EtGly: C, 55.83; H, 3.22; N 8.14. Found C, 56.59, H, 3.84; N 8.34. The observed differences could be related to the small masses of the **1**·MeOH and **1**·EtOH samples, less than 1 mg, used for the analysis.

S2.2 Crystal structures

Table S1: Crystallographic, data collection and refinement data for **1**·EtOH and **1**·MeOH.

Compound	**1**·EtOH@100K	**1**·EtOH@RT	**1**·MeOH@100K	**1**·MeOH@RT
Empirical formula	$C_{32}H_{22}Cl_2CoN_4O_5$	$C_{32}H_{22}Cl_2CoN_4O_5$	$C_{31}H_{20}Cl_2CoN_4O_5$	$C_{31}H_{20}Cl_2CoN_4O_5$
Formula wt. / g mol^{-1}	672.36	672.36	658.34	658.34
Colour	red	red	red	red
Crystal dimensions / mm	0.33 x 0.09 x 0.04	0.34 x 0.08 x 0.04	0.43 x 0.13 x 0.11	0.32 x 0.12 x 0.08
Space group	$P2_1/n$	$C2/c$	$C2/c$	$C2/c$
a / Å	12.5057(1)	12.3227(2)	12.2252(2)	12.3162(1)
b / Å	14.7939(1)	15.5712(2)	14.9241(3)	15.0215(1)
c / Å	16.3923(2)	16.4092(2)	16.2146(3)	16.4187(1)
α / °	90	90	90	90
β / °	111.624(1)	111.845(2)	111.767(2)	111.838(1)
γ / °	90	90	90	90
Z	4	4	4	4
V / Å^3	2819.27(5)	2922.50(8)	2747.42(9)	2819.61(4)
D_{calc} / g cm^{-3}	1.584	1.528	1.584	1.544
λ / Å	1.54179 (CuKα)	1.54179 (CuKα)	1.54179 (CuKα)	1.54179 (CuKα)
μ / mm^{-1}	6.950	6.704	7.118	6.936
Θ range / °	3.84 – 97.95	4.80 – 79.42	4.89 - 79.68	4.86 - 79.73
T / K	100(2)	293(2)	100(2)	293(2)
Diffractometer type	Synergy S	Synergy S	Synergy S	Synergy S
Range of h, k, l	-15 < h < 15; -18 < k < 18; -20 < l < 16	-15 < h < 15; -18 < k < 19; -20 < l < 17	-15 < h < 15; -19 < k < 18; -19 < l < 20	-14 < h < 15; -18 < k < 19; -20 < l < 19
Reflections collected	23581	11552	10791	23431
Independent reflections	6001	3084	2908	3055
Observed reflections ($I \geq 2\sigma$)	5673	2758	2810	2975
Absorption correction	Gaussian	Gaussian	Gaussian	Gaussian
T_{min}, T_{max}	0.539; 1.000	0.511; 1.0000	0.411; 1.000	1.000; 0.495
R_{int}	0.0326	0.0394	0.0392	0.0384
$R(F)$	0.0352	0.0417	0.0350	0.0319
$R_w(F^2)$	0.1043	0.1253	0.0959	0.0905
Goodness of fit	1.074	1.022	1.059	1.085
H atom treatment	Constrained	Constrained	Constrained	Constrained
No. of parameters	397	213	201	206
No. of restraints	0	16	1	9
$\Delta\rho_{max}$, $\Delta\rho_{min}$ (eÅ^{-3})	0.701; -0.532	0.220; -0.459	0.644; -0.400	0.194; -0.408

Table S2: Crystallographic, data collection and refinement data for **1**·EtGly.

Compound	**1**·EtGly@100K	**1**·EtGly@RT
Empirical formula	$C_{32}H_{22}Cl_2CoN_4O_6$	$C_{32}H_{22}Cl_2CoN_4O_6$
Formula wt. / g mol^{-1}	688.36	688.36
Colour	red	red
Crystal dimensions / mm	0.29 x 0.07 x 0.05	0.29 x 0.07 x 0.05
Space group	*C* 2/*c*	*C* 2/*c*
a / Å	12.4721(4)	12.3226(3)
b / Å	14.9085(4)	15.5674(3)
c / Å	16.3578(4)	16.4143(3)
α / °	90	90
β / °	111.904(3)	111.865(2)
γ / °	90	90
Z	4	4
V / Å^3	2822.00(15)	2922.26(11)
D_{calc} / g cm^{-3}	1.620	1.560
λ / Å	1.54179 (Cu*K*α)	1.54179 (Cu*K*α)
μ / mm^{-1}	6.986	6.746
Θ range / °	4.84 – 79.48	4.80 – 79.58
T / K	100(2)	293(2)
Diffractometer type	Synergy S	Synergy S
Range of *h*, *k*, *l*	$-15 < h < 15$; $-16 < k < 18$; $-20 < l < 15$	$-15 < h < 15$; $-19 < k < 19$; $-17 < l < 20$
Reflections collected	9613	12600
Independent reflections	2938	3121
Observed reflections ($I \geq 2\sigma$)	2550	2856
Absorption correction	Gaussian	Gaussian
T_{min}, T_{max}	0.585; 1.000	0.603; 1.000
R_{int}	0.0575	0.0262
R (F)	0.0703	0.0487
R_w (F^2)	0.2052	0.1588
Goodness of fit	1.069	1.056
H atom treatment	Constrained	Constrained
No. of parameters	204	187
No. of restraints	0	0
$\Delta\rho_{max}$, $\Delta\rho_{min}$ (eÅ^{-3})	0.542; -0.959	0.454; -0.471

Table S3: Bond lengths in the chloranilate anion (Å). Symmetry operator: *i*) -*x*, *y*, -*z*+1/2.

	1·EtGly@RT	**1·EtGly@100K**	**1·MeOH@RT**	**1·MeOH@100K**	**1·EtOH@RT**
C1 - C2	1.377(3)	1.369(6)	1.380(2)	1.382(3)	1.383(3)
C2 - C3	1.418(4)	1.416(6)	1.415(2)	1.416(3)	1.410(3)
C3 - C3^{i}	1.546(5)	1.550(7)	1.549(3)	1.234(2)	1.547(4)
C1 - C1^{i}	1.534(3)	1.539(5)	1.527(2)	1.529(3)	1.527(3)
C1 - O1	1.263(3)	1.269(5)	1.2661(17)	1.266(2)	1.263(3)
C3 - O2	1.227(3)	1.233(6)	1.232(2)	1.234(2)	1.233(3)
C2 - Cl1	1.737(3)	1.744(4)	1.7371(18)	1.745(2)	1.737(2)
	1· EtOH@100K				
C1 - C2	1.531(2)				
C2 - C3	1.386(2)				
C3 - C4	1.420(2)				
C4 - C5	1.553(3)				
C5 - C6	1.418(2)				
C6 - C1	1.384(2)				
C1 - O1	1.2682(18)				
C2 - O2	1.2659(19)				
C4 - O3	1.232(2)				
C5 - O4	1.236(2)				
C3 - Cl1	1.7391(18)				
C6 - Cl2	1.7414(18)				

Table S4: Aromatic stacking geometry parameters.

a) Analysis of short ring-interactions with Cg(*i*)···Cg(*j*) distances < 4.0 Å and β < 60.0° for compounds **1**·MeOH, **1**·EtOH and **1**·EtGly at 100K.

Compound	Cg(*i*)···Cg(*j*)	Cg(*i*)···Cg(*j*)/Å[a]	α/°[b]	β/°[c]	Cg(*i*)···plane [Cg(*j*)]/Å	Symmetry operator
1·MeOH	(N2→C13)···(N2→C13)	3.8329(11)	0.00(9)	25.7	3.4527(8)	1-X,Y,1/2-Z
	(N2→C13)···(C7→C14)	3.6059(12)	18.3	17.1	3.4464(8)	3/2-X,1/2-Y,1-Z
1·EtOH	(N2→C16)···(N3→C23)	3.8547(9)	3.07(8)	26.5	3.4192(7)	1/2+X,3/2-Y,1/2+Z
	(N2→C16)···(C22→C29)	3.5796(10)	4.06(8)	21.2	3.4202(7)	1/2+X,3/2-Y,1/2+Z
	(N3→C23)···(C10→C17)	3.6585(10)	1.94(8)	18.2	3.4417(7)	-1/2+X,3/2-Y,-1/2+Z
1·EtGly	(N1→C8)···(N1→C8)	3.835(3)	0.0(2)	26.7	3.427(3)	1/2-X,3/2-Y,1-Z
	(N1→C8)···(C7→C14)	3.606(3)	1.5	19.7	3.423(2)	1/2-X,3/2-Y,1-Z

[a] Cg = centre of gravity of the aromatic ring. [b] α = angle between the planes of two aromatic rings. [c] β = angle between the Cg···Cg line and the normal to the plane of the first aromatic ring.

b) Analysis of Y–X···Cg (π-ring) interactions (H···Cg(*j*) < 3.0 Å or X···Cg(*j*) < 4.0 Å; and γ < 30.0°) for compounds **1**·MeOH, **1**·EtOH and **1**·EtGly at 100K.

Compound	Y–X···Cg(*j*)	X···Cg(*j*)/Å[a]	γ/°[b]	Y–X···Cg(*j*)/°[c]	Y···Cg(*j*)/Å	Y–X, π /°[d]	Symmetry operator
1·MeOH	C2–Cl1···(N1→C8)	3.6566(9)	19.03	113	4.638(7)	41.98	1/2+X,1/2+Y,Z
	C2–Cl1···(C7→C14)	3.6980(10)	21.07	151	5.301(2)	41.60	1/2+X,1/2+Y,Z
	O3–C16···(N2→C13)	3.6620(8)	10.52	152	4.927(4)	72.34	1-X,1+Y,1/2-Z
1·EtOH	C3–Cl1···(N4→C28)	3.4885(8)	16.99	118	4.5829(18)	44.56	3/2-X,-1/2+Y,3/2-Z
	C3–Cl1···(C22→C29)	3.6903(8)	25.64	157	5.3353(19)	43.95	3/2-X,-1/2+Y,3/2-Z
	C6–Cl2···(N1→C11)	3.7550(8)	16.30	144	4.7479(18)	38.26	1/2-X,-1/2+Y,3/2-Z
	C6–Cl2···(C10→C17)	3.9835(8)	25.56	150	5.5630(19)	37.70	1/2-X,-1/2+Y,3/2-Z
1·EtGly	C2–Cl1···(N1→C8)	3.655(2)	17.87	115	4.687(5)	42.15	-1/2+X,-1/2+Y,Z
	C2–Cl1···(C7→C14)	3.810(2)	24.44	153	5.423(4)	41.50	-1/2+X,-1/2+Y,Z

[a] Cg(*j*) = centre of gravity of the aromatic (π) ring. [b] γ = angle between Cg(*j*)–X vector and ring Cg(*j*) normal. [c] = angle of the Y–X bond with the π -plane (i.e. Perpendicular = 90°, Parallel = 0°).

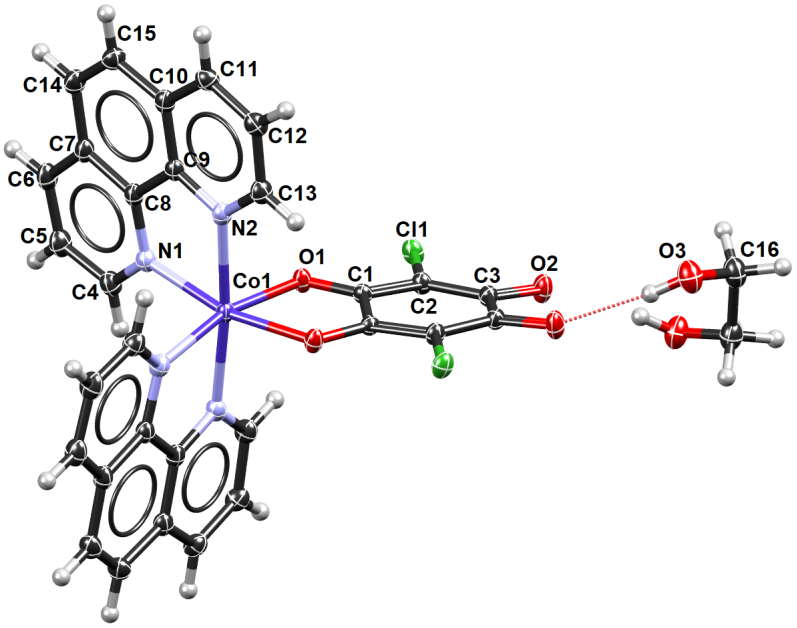

Figure S1: ORTEP-3 drawing of **1**·EtGly at 100 K with atom numbering scheme. Displacement ellipsoids are drawn for the probability of 50 % and hydrogen atoms are shown as spheres of arbitrary radii.

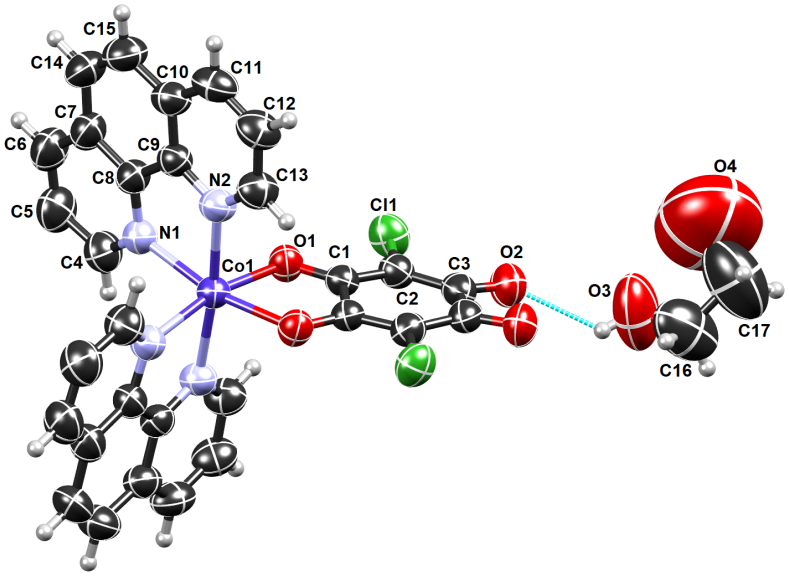

Figure S2: ORTEP-3 drawing of **1**·EtGly at RT with atom numbering scheme. Displacement ellipsoids are drawn for the probability of 50 % and hydrogen atoms are shown as spheres of arbitrary radii.

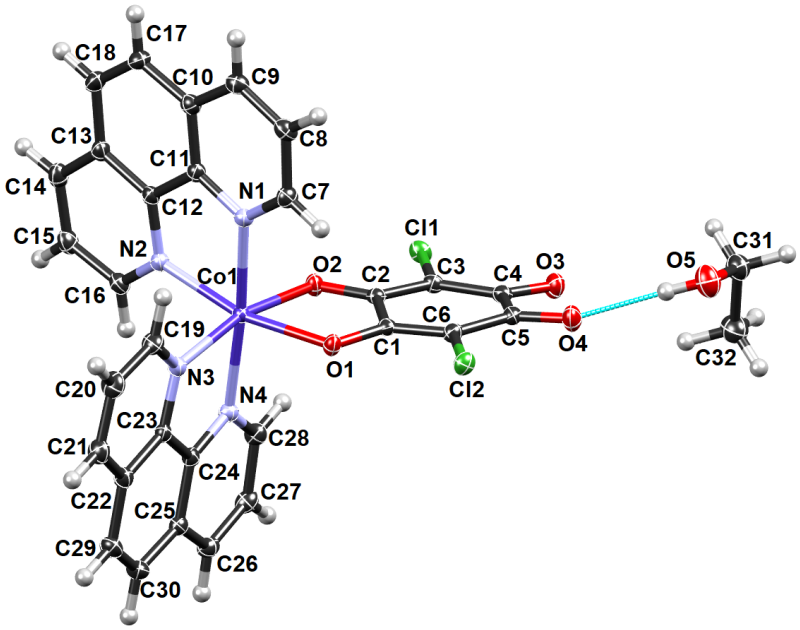

Figure S3: ORTEP-3 drawing of **1**·EtOH at 100 K with atom numbering scheme. Displacement ellipsoids are drawn for the probability of 50 % and hydrogen atoms are shown as spheres of arbitrary radii. Only one component of the disorder is shown.

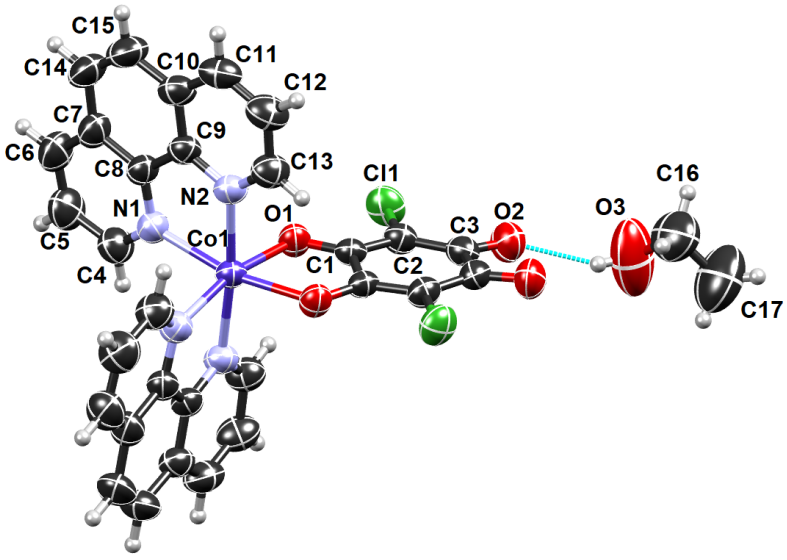

Figure S4: ORTEP-3 drawing of **1**·EtOH at RT with atom numbering scheme. Displacement ellipsoids are drawn for the probability of 50 % and hydrogen atoms are shown as spheres of arbitrary radii.

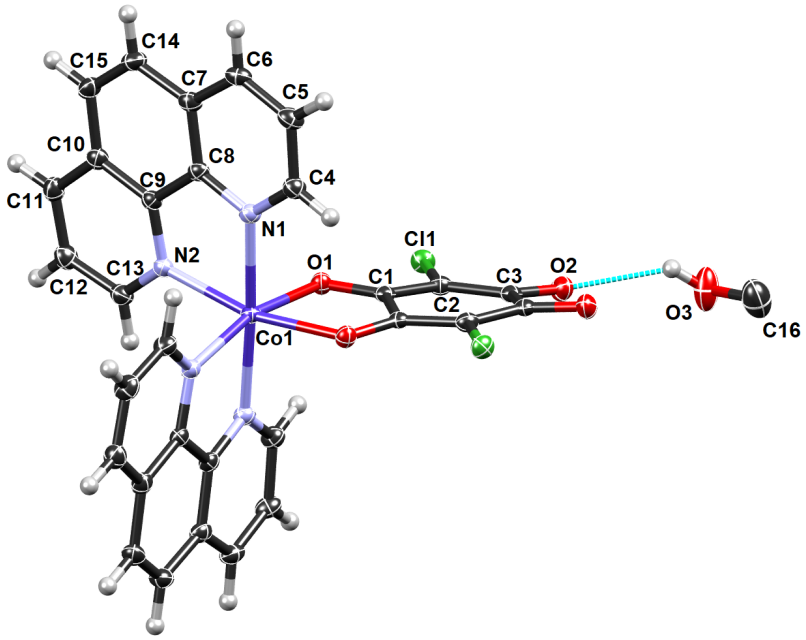

Figure S5: ORTEP-3 drawing of **1**·MeOH at 100 K with atom numbering scheme. Displacement ellipsoids are drawn for the probability of 50 % and hydrogen atoms are shown as spheres of arbitrary radii.

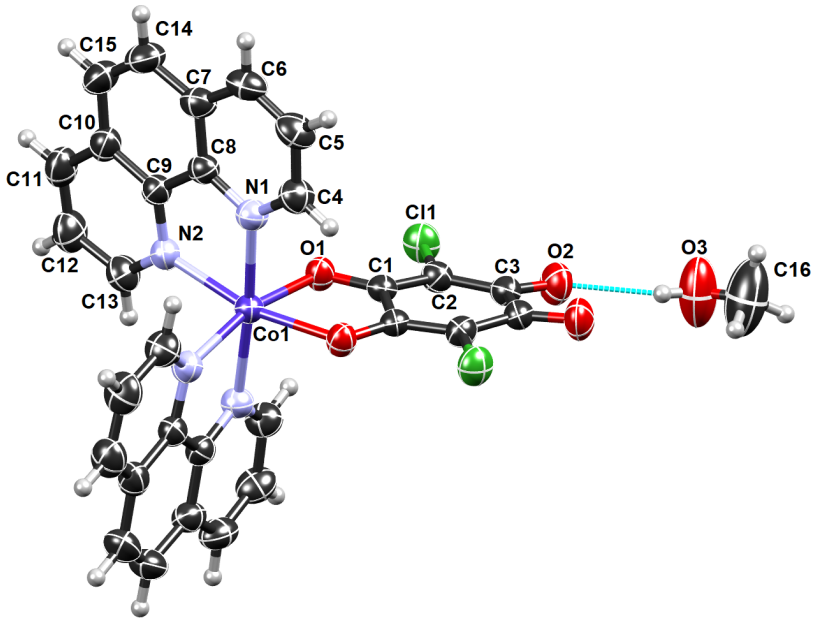

Figure S6: ORTEP-3 drawing of **1**·MeOH at RT with atom numbering scheme. Displacement ellipsoids are drawn for the probability of 50 % and hydrogen atoms are shown as spheres of arbitrary radii.

S2.3 Powder X-ray diffraction

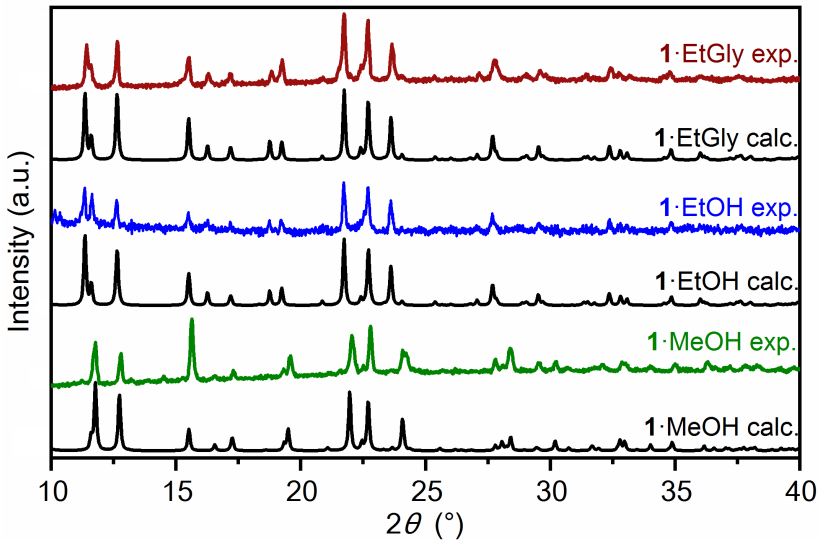

Figure S7: PXRD patterns of cobalt(II)-phenanthroline compounds with chloranilic acid: **1**·MeOH, **1**·EtOH and **1**·EtGly. The experimental data (colored lines) are confirmed by calculated PXRD patterns from single-crystal XRD data (black lines).

S2.4 Magnetization study

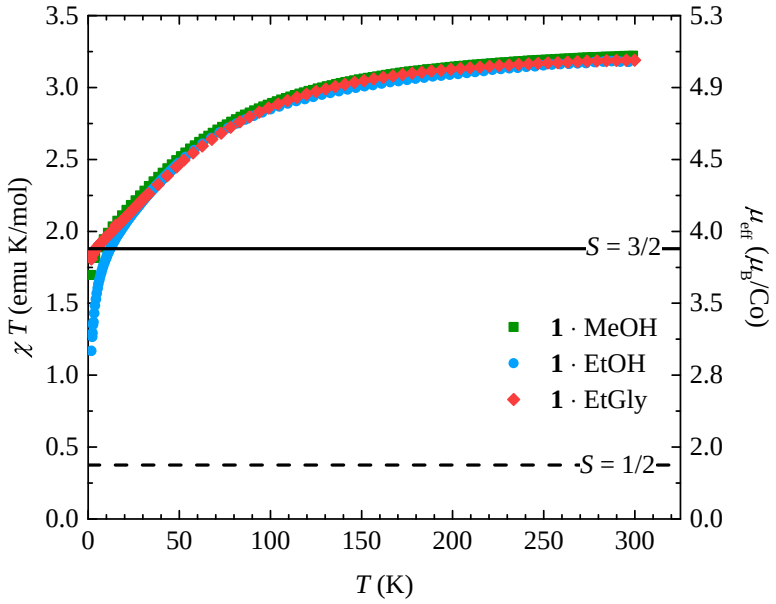

Figure S8: Temperature dependence of χT (left y-axis) and effective magnetic moment μ_{eff} (right y-axis) measured for the three complexes **1**·MeOH, **1**·EtOH and **1**·EtGly in $\mu_0 H = 0.1$ T.

S2.5 Magnetic modeling

Magnetic susceptibility data were corrected by the diamagnetic contribution of the capsule ($2{\cdot}10^{-6}$ emu in 1000 Oe) and sample's diamagnetic contribution according to the Pascal formula. Additionally, Hamiltonian (5) takes g values for the free electron, g_e=2.0023, as fixed values. Fitting and all the other calculations were done using own developed code in Python 3.9 using scipy.optimize.leastsq for optimization with the advantages mentioned in the main text. Mean susceptibility is calculated as mean magnetization devided by the applied magnetic field. Mean magnetization is calculated exactly according to the physical expression for magnetization:

$$M = \frac{N\sum_n(-\partial E_n/\partial B)\exp\left(\frac{-E_n}{kT}\right)}{\sum_n \exp\left(\frac{-E_n}{kT}\right)} \tag{S4}$$

Where E_n (n = 1,2,3..) is an energy spectrum in the presence of the applied magnetic field B. This is accounted for every direction of the magnetic field given in the spherical coordination system: $B_u = B(sin(\theta)cos(\phi), sin(\theta)sin(\phi), cos(\theta))$. Magnetization is then calculated aggregate over all directions:

$$M = \frac{1}{4\pi}\int\int M_u sin(\theta) d\theta d\phi \tag{S5}$$

The integral is calculated numerically over 81 equally distributed directions using the numerical Simpson integral algorithm. To avoid it to be completely slow, at each temperature, magnetization for each direction should be calculated first and those values stored. Then, for each temperature integral is calculated fast with the stored values.

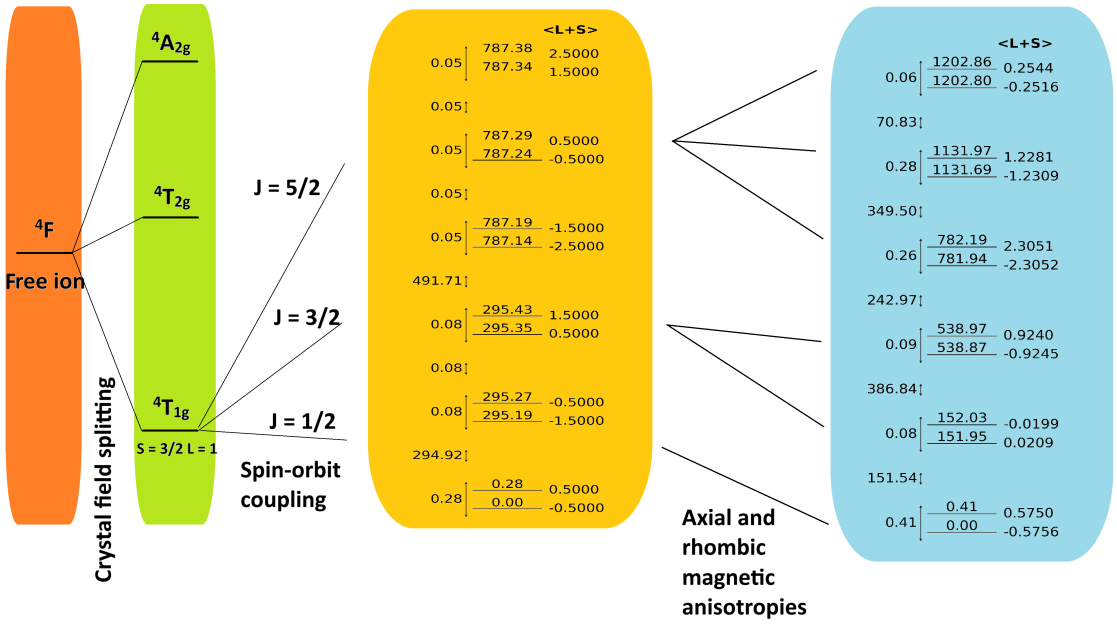

Figure S9: Energy diagram showing splitting of the free ion ^4F term in octahedral crystal field by spin-orbit coupling and magnetic anisotropies for **1**·EtOH complex calculated for fit parameters for magnetic field of 1000 Oe parallel to z magnetic axis. Energies in cm^{-1} are written on solid lines that represent energy levels. On the left and right sides of the energy levels, the energy gap and the corresponding total spin $J = L + S$ for each energy level are given, respectively.

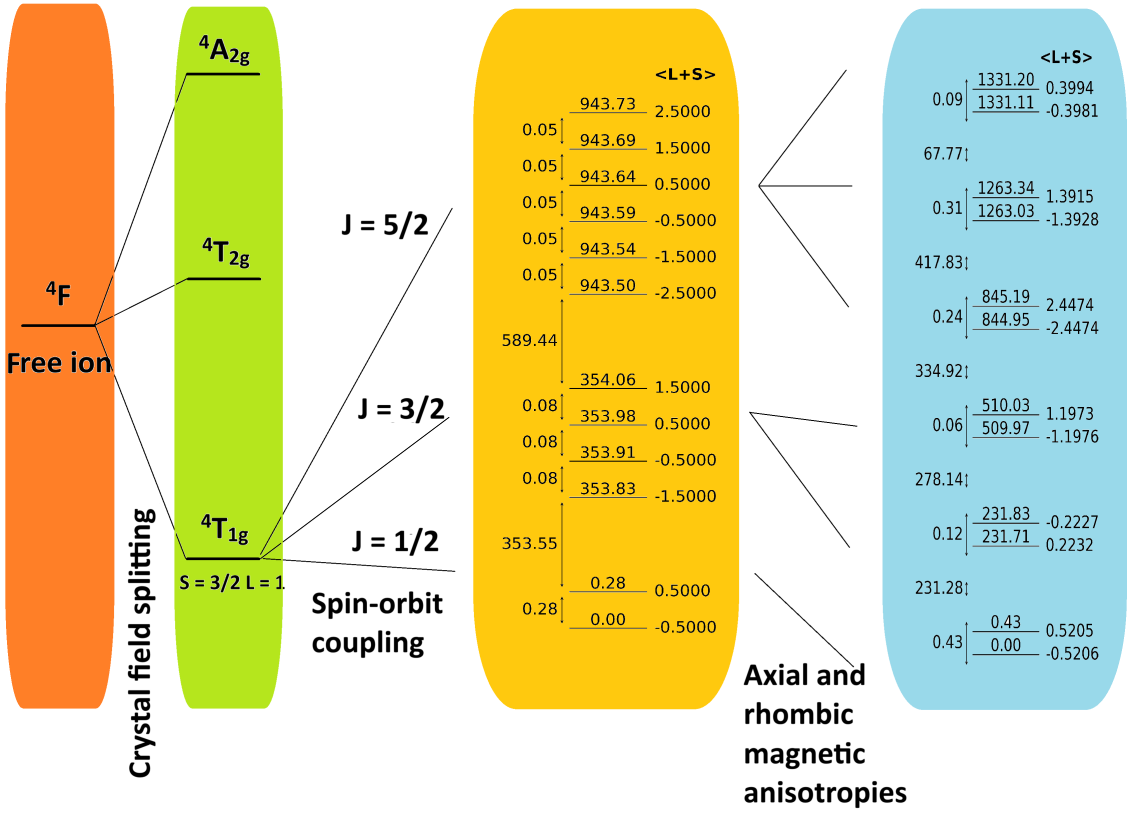

Figure S10: Energy diagram showing splitting of the free ion ^4F term in octahedral crystal field by spin-orbit coupling and magnetic anisotropies for **1**·EtGly complex calculated for fit parameters for magnetic field of 1000 Oe parallel to z magnetic axis. Energies in cm^{-1} are written on solid lines that represent energy levels. On the left and right sides of the energy levels, the energy gap and the corresponding total spin $J = L + S$ for each energy level are given, respectively.

S2.6 AC magnetic susceptibility

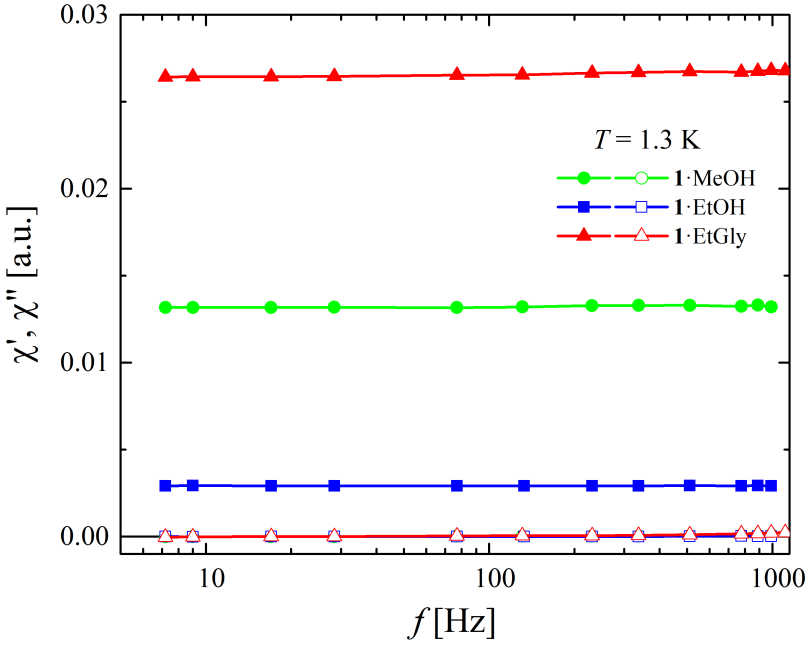

Figure S11: In-phase χ' (full symbols) and out-of-phase χ'' (open symbols) component of ac magnetic susceptibility measured at 1.3 K without external static magnetic field for samples **1**·MeOH, **1**·EtOH and **1**·EtGly.

S2.7 DFT study

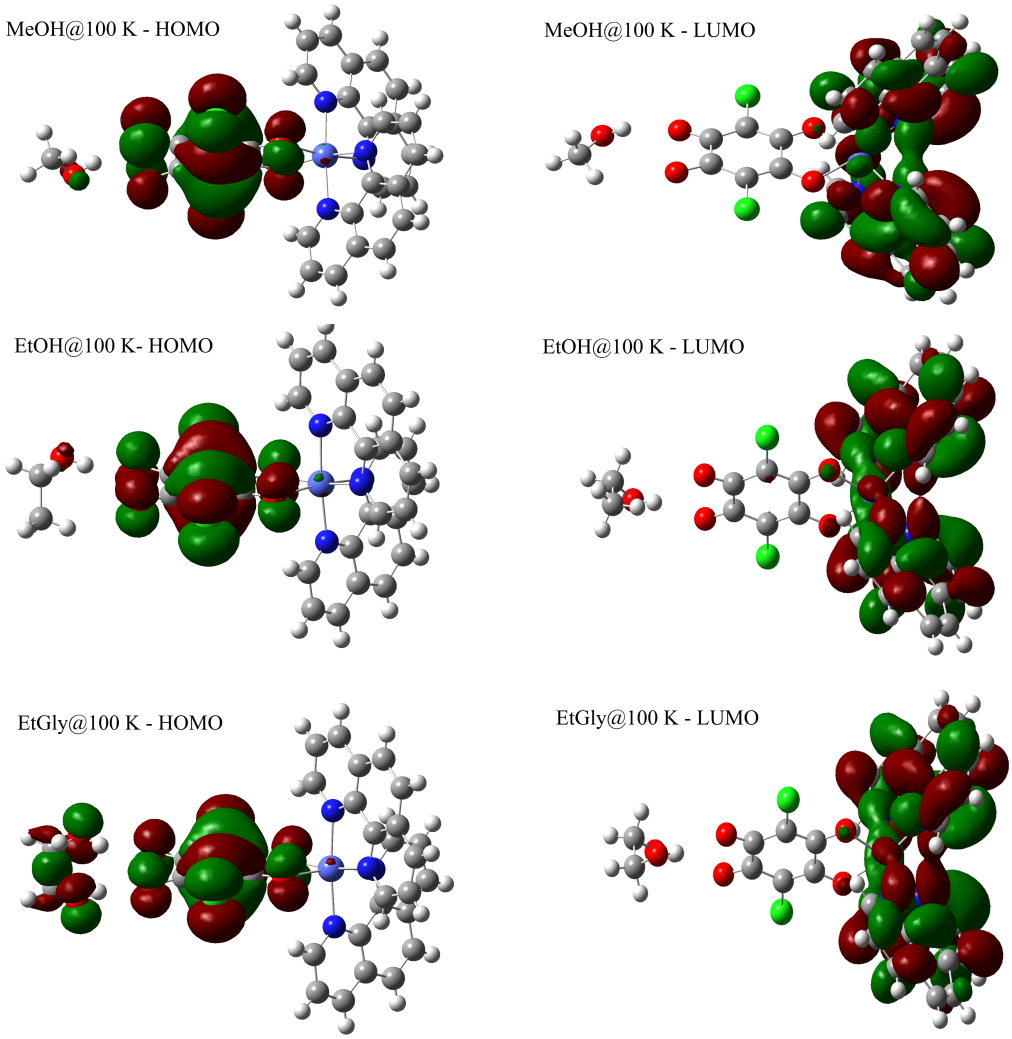

Figure S12: Delocalization of frontier molecular orbitals for the quartet ($S = 3/2$) states as obtained from the DFT calculations at B3LYP/LANL2DZ level of theory, HOMO here refers to the highest singly occupied state and LUMO to the lowest unoccupied state. The values of the orbital energies are as follows: $E_{HOMO} = -4.41$ eV, $E_{LUMO} = -3.04$ eV for **1**·MeOH, $E_{HOMO} = -4.38$;eV, $E_{LUMO} = -3.03$ eV for **1**·EtOH and $E_{HOMO} = -4.55$ eV, $E_{LUMO} = -3.08$ eV for **1**·EtGly.

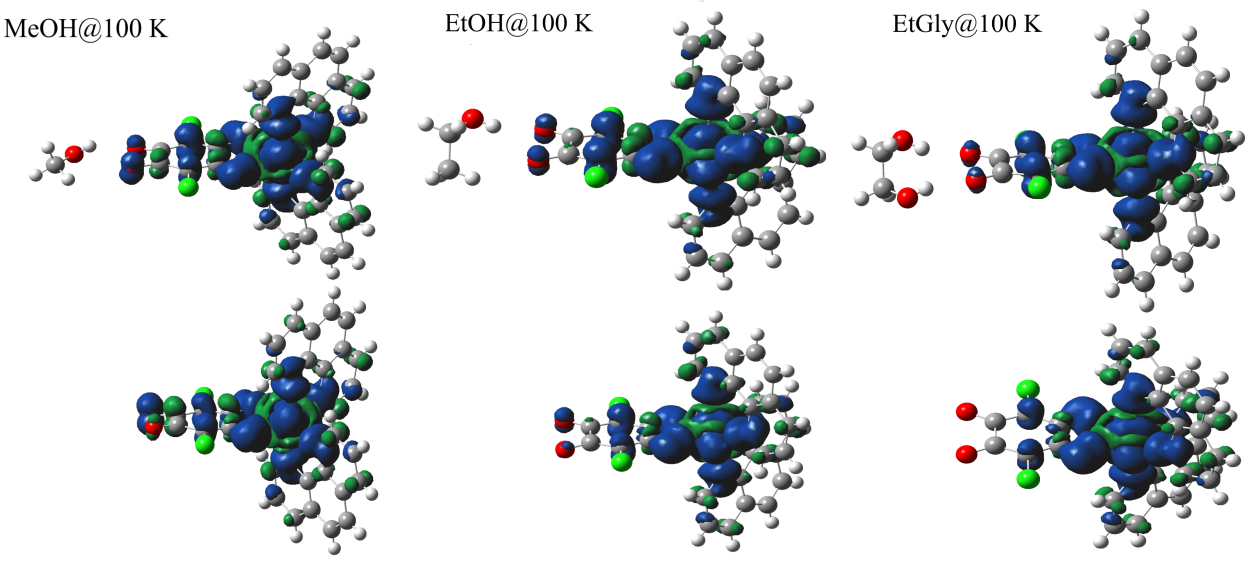

Figure S13: Spin density distribution for the quartet ($S = 3/2$) states in presence of the solvent molecules (upper panels) and without solvent molecules (lower panels), as obtained from the DFT calculations at B3LYP/LANL2DZ level of theory. Blue color represents the spin up (α), while the green color spin down (β) electron density, respectively.

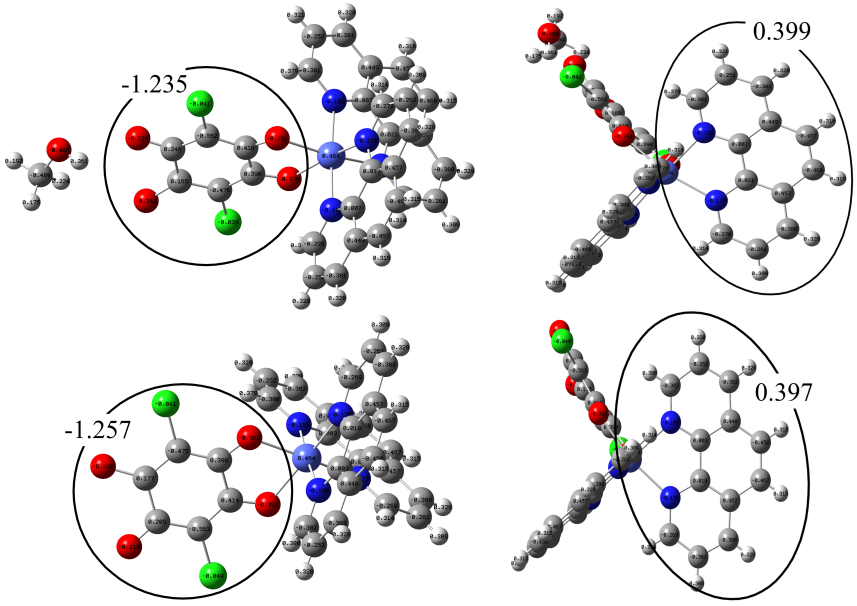

Figure S14: Mulliken atomic charges in presence of the solvent molecules (upper panels) and without solvent molecules (lower panels) for the case of MeOH, as obtained from the DFT calculations at B3LYP/LANL2DZ level of theory. The partial electric charges are printed on each atom and the sum of the partial charges of the atoms in the ligands (the chloranilate ligand and one of the phenanthroline ligands) is shown in the figure.

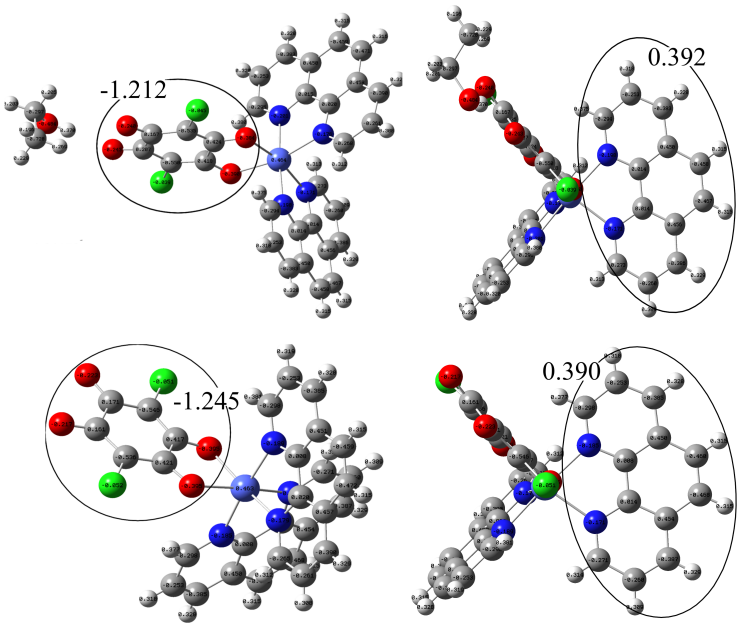

Figure S15: Mulliken atomic charges in presence of the solvent molecules (upper panels) and without solvent molecules (lower panels) for the case of EtOH, as obtained from the DFT calculations at B3LYP/LANL2DZ level of theory. The partial electric charges are printed on each atom and the sum of the partial charges of the atoms in the ligands (the chloranilate ligand and one of the phenanthroline ligands) is shown in the figure.

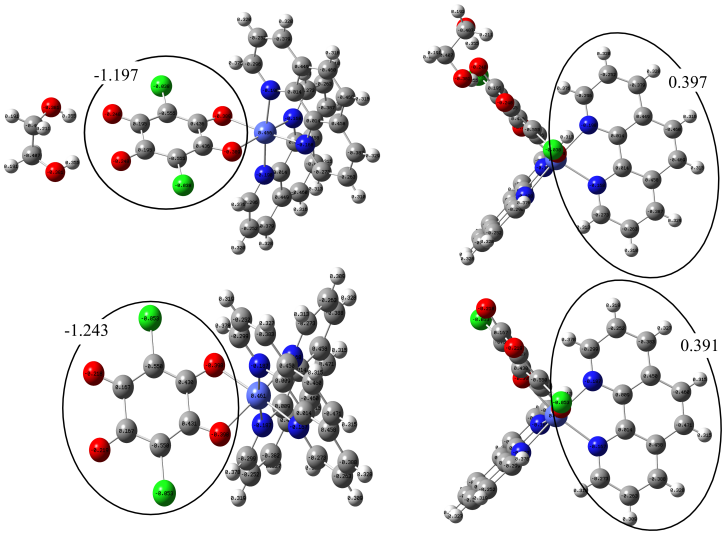

Figure S16: Mulliken atomic charges in presence of the solvent molecules (upper panels) and without solvent molecules (lower panels) for the case of EtGly, as obtained from the DFT calculations at B3LYP/LANL2DZ level of theory. The partial electric charges are printed on each atom and the sum of the partial charges of the atoms in the ligands (the chloranilate ligand and one of the phenanthroline ligands) is shown in the figure.

References

[1] O. D. Rigaku, *P.R.O. CrysAlis, version: 1.171.39.46*, Rigaku oxford diffraction ltd, Yarnton, Oxfordshire, England technical report, 2018.

[2] G. M. Sheldrick, *SHELXT* – Integrated space-group and crystal-structure determination, *Acta Crystallogr. A*, 2015, **71**, 3–8.

[3] G. M. Sheldrick, Crystal structure refinement with *SHELXL*, *Acta Crystallogr. C*, 2015, **71**, 3–8.

[4] A. L. Spek, *checkCIF* validation ALERTS: what they mean and how to respond, *Acta Crystallogr. E*, 2020, **76**, 1–11.

[5] L. J. Farrugia, *J. Appl. Crystallogr.*, 1997, **30**, 565.

[6] C. F. Macrae, I. Sovago, S. J. Cottrell, P. T. A. Galek, P. McCabe, E. Pidcock, M. Platings, G. P. Shields, J. S. Stevens, M. Towler and P. A. Wood, *Mercury 4.0*: from visualization to analysis, design and prediction, *J. Appl. Crystallogr.*, 2020, **53**, 226–235.

[7] R. Ketkaew, Y. Tantirungrotechai, P. Harding, G. Chastanet, P. Guionneau, M. Marchivie and D. J. Harding, OctaDist: a tool for calculating distortion parameters in spin crossover and coordination complexes, *Dalton Transactions*, 2021, **50**, 1086–1096.

[8] M. J. e. a. Frisch, *Gaussian 09*, 2009, Gaussian, Inc., Wallingford CT.